Journal of Materiomics 7 (2021) 545–555

Contents lists available at ScienceDirect

Journal of Materiomics

journal homepage: www.journals.elsevier.com/journal-of-materiomics/

Sb_2Te_3/graphite nanocomposite: A comprehensive study of thermal conductivity

Subarna Das [a, b], P. Singha [a], V.A. Kulbachinskii [c, d], V.G. Kytin [c], Gangadhar Das [e], S. Janaky [e], A.K. Deb [f], Sudip Mukherjee [g], A. Maignan [b], S. Hebert [b], R. Daou [b], Chandrabhas Narayana [e], S. Bandyopadhyay [a, h], Aritra Banerjee [a, h, *]

[a] Department of Physics, University of Calcutta, 92 A P C Road, Kolkata, 700 009, India
[b] Laboratoire de Cristallographie et Sciences des Matériaux (CRISMAT), Normandie Université, UMR6508 CNRS, ENSICAEN, UNICAEN, 14000, Caen, France
[c] Department of Low Temperature Physics and Superconductivity, Physics Faculty, M.V. Lomonosov Moscow State University, 119991, Moscow, Russia
[d] Moscow Institute of Physics and Technology, 141700, Dolgoprudny, Moscow Region, Russia
[e] Chemistry and Physics of Materials Unit, Jawaharlal Nehru Centre for Advanced Scientific Research, Jakkur P.O, Bangalore, 560 064, India
[f] Department of Physics, Raiganj University, Uttar Dinajpur, West Bengal, 733 134, India
[g] UGC-DAE Consortium for Scientific Research, Mumbai Centre, R-5 Shed, BARC Campus, Trombay, Mumbai, 400 008, India
[h] Center for Research in Nanoscience and Nanotechnology, University of Calcutta, JD-2, Sector-III, Saltlake, Kolkata, 700 106, India

ARTICLE INFO

Article history:
Received 23 September 2020
Received in revised form
17 November 2020
Accepted 26 November 2020
Available online 3 December 2020

Keywords:
Thermoelectric systems
Thermal conductivity
Phonons
X-ray powder diffraction
Raman spectroscopy
Specific heat measurements

ABSTRACT

Thermoelectric performance largely depends on the reduction of lattice thermal conductivity (κ_L). The study of the thermal conductivity (κ) of a Sb_2Te_3/graphite nanocomposite system demonstrates ~40% reduction in κ_L with graphite incorporation. A plausible explanation of intrinsic low κ_L observed in Sb_2Te_3 based system is presented by modeling experimental specific heat (C_p) data. Raman spectroscopy measurement combined to X-Ray diffraction data confirms the presence of graphite as separate phase in the composite sample. It is found that phonon scattering dominates heat transport mechanism in the nanostructured Sb_2Te_3/graphite composite. Large reduction in κ_L is accomplished by intensifying scattering rate of phonons via various sources. Graphite introduces effective scattering sources, *i.e.*, defects of different dimensionalities in synthesized nanocomposite sample. Furthermore, graphite mediates phonon-phonon coupling and enhances lattice anharmonicity, which causes an intrinsic scattering of phonons with all frequencies in the Sb_2Te_3/graphite nanocomposite sample. Dislocation density and phonon anharmonicity of the synthesized samples are estimated from in depth analysis of temperature dependent synchrotron powder diffraction and Raman spectroscopic data. κ_L value as low as 0.8 W $m^{-1}K^{-1}$ at 300 K, achieved with graphite dispersion in Sb_2Te_3 based composite system makes the present comprehensive study an interesting concept to be developed in thermoelectric materials.

1. Introduction

Thermoelectric (TE) materials have the potential to play a significant role in converting a part of waste heat to useable electrical energy. Materials with intrinsically low thermal conductivity (κ) are of practical interest [1]. In principle, charge carriers, phonons, photons, excitons, magnons can all contribute to heat transport and thus to κ in a material. But in potential TE materials, κ mostly consists of electronic part (κ_e) and lattice/phonon part (κ_L) with $\kappa_e < \kappa_L$ [2,3]. Lattice thermal conductivity (κ_L) is the only independent tunable parameter in TE Figure of merit ZT ($=\frac{S^2}{\rho\kappa}T$) where S, ρ and T are the Seebeck coefficient, electrical resistivity and absolute temperature respectively [4–6]. Hence, reduction in κ_L has been a point of great interest in order to improve the efficiency of TE materials, ZT [3,7–11].

Intensifying phonon scattering, *i.e.*, shortening phonon relaxation time (τ) is a promising strategy for achieving low κ_L. Heat carrying phonons have a broad spectrum of frequencies. Different scattering sources have their own frequency (ω) dependence. Grain boundaries (2D defects) can effectively scatter low-frequency phonons ($\tau_B \propto \omega^0$), high frequency phonons are mostly targeted

* Corresponding author. Department of Physics, University of Calcutta, 92 A P C Road, Kolkata, 700 009, India.
E-mail address: arbphy@caluniv.ac.in (A. Banerjee).
Peer review under responsibility of The Chinese Ceramic Society.

https://doi.org/10.1016/j.jmat.2020.11.014

by point defects (0D defects) with $\tau_{PD} \propto \omega^{-4}$ [8,9]. Nano or meso structuring would lead to grain boundary engineering, while alloying has been demonstrated as an effective route for modulating point defect [3,7,12]. On the other hand, dislocation strain fields ($\tau_{DS} \propto \omega^{-1}$) and dislocation cores ($\tau_{DC} \propto \omega^{-3}$) are suitable scattering centers for phonons of mid-frequency (1D defects). Kim et al. demonstrated the role of dislocation arrays formed at grain boundaries in lowering κ_L of $Bi_{0.5}Sb_{1.5}Te_3$ [8]. κ_L as low as 0.4 W $m^{-1}K^{-1}$ is also reported to be achieved by engineering vacancy induced dislocations within grains of PbSe thermoelectrics [9]. In addition, strong anharmonicity in lattice vibration increases phonon-phonon scattering through Umklapp (τ_U) and normal (τ_N) processes ($\tau_{U,N} \propto \omega^{-2}$), which is helpful to scatter phonons of all frequency [13–15]. All the scattering mechanisms contribute collectively to shorten total phonon relaxation time (τ_{total}) and hence decrease κ_L [8,9].

Many of the recent successes in lowering κ_L and hence increasing TE performance have been achieved through composites [16–19], consisting of TE matrix and nanoscale constituents. Low energy charge carriers get filtered in the nanograin boundaries of the composite leading to increase of *S*. Newly formed heterointerfaces of TE matrix and dispersoids scatter phonons more effectively than charge carriers leading to decrease of κ without much compromise to ρ [12,20,21]. There have been reports of κ_L reduction in some well-known TE materials like PbTe, SnTe, SnSe, Bi_2Te_3 through composite route [21–29]. Due to its potential for near room temperature application, Sb_2Te_3, possessing layered crystal structure, is a popular TE material with intrinsically low κ_L [14,30–32]. Very limited efforts have been made to further lower its κ_L through composite approach [19,33,34]. Lee et al. have reported a low κ_L value of 1.4 W $m^{-1}K^{-1}$ in Ag_2Te incorporated Sb_2Te_3 composite [34]. However, despite such attempts, underlying mechanism and effect of different type of material defects on phonon scattering in composite systems is still elusive in nature. It is also noteworthy to mention here that understanding of phonon dynamics and its relation with the lowering of κ_L in composite TE systems, which is absolutely critical for further enhancement of TE performance, remains unexplored so far.

We herein report ~40% decrease of κ_L in Sb_2Te_3/graphite nanocomposite system as compared to its pristine counterpart and have attempted to investigate the role of phonon dynamics in details. Carbon based materials are effective in phonon blocking [16]. The thermal property of graphite, which possesses layered structured, is highly anisotropic [35,36]. In addition graphite is a light ecofriendly material with high electrical in-plane conductivity, high carrier mobility and excellent mechanical properties [35]. These properties encourage us to choose graphite as a possible disperoid in the Sb_2Te_3 matrix. Interestingly, in this composite system when the wt% of graphite is lower than 1%, its Seebeck coefficient is keeping an unchanged value as compared to the graphite free analogue [36] which allows to study κ in samples having the same charge carrier concentrations. In the following, we report on the role of graphite addition on scattering phonons of entire frequency spectrum by various scattering sources, *viz.*, point defects (0D defects), dislocation type defects (1D defects), grain boundary and Sb_2Te_3/graphite heterointerfaces (2D defects). Both the microscopic characterization based on temperature-dependent synchrotron radiation diffraction and Raman spectroscopic measurements and macroscopic characterization by specific heat (C_p) measurement of nanostructured Sb_2Te_3/graphite composite system have been performed. Dislocation density in the samples has been calculated by modified Williamson Hall method. Phonon anharmonicity is estimated through temperature dependent synchrotron X-ray, Raman spectroscopic and C_p data. This reveals that anharmonicity arising due to lattice thermal expansion is higher in pristine Sb_2Te_3 sample. But high phonon-phonon coupling in Sb_2Te_3/graphite ensures an overall increase of phonon anharmonicity in graphite incorporated composite sample. Finally, the obtained clues to low κ_L related to phonon scattering mechanism and anharmonic lattice vibration are discussed.

2. Experiments

To prepare the Sb_2Te_3 + x wt% graphite (x = 0, 0.5) nanocomposite samples, polycrystalline Sb_2Te_3 ingot was initially synthesized by solid state reaction method [14]. To obtain corresponding Sb_2Te_3/graphite nanocomposite samples, desired weight percentage of graphite was added with synthesized Sb_2Te_3 ingots and ball milled, the details of which can be found in supplementary material. Hot pressed pellets of Sb_2Te_3 + x wt% graphite samples were used for κ measurement [37]. Low-temperature (15–300 K) powder X-ray Diffraction (XRD) experiments were carried out using the synchrotron radiation facility at Indian beamline BL-18B, Photon Factory, KEK, Japan. X-ray beam of wavelength $\lambda = 0.9782$ Å was selected for illuminating the samples. For detailed structural characterization, Rietveld refinement of the synchrotron X-ray patterns was performed using MAUD software [38,39]. The microstructural refinement according to the formalism of Popa [40] is capable of modeling both isotropic and anisotropic size and strain broadening. This has been used in the present Rietveld analysis. It is noteworthy to mention that during refinement of Sb_2Te_3 + 0.5 wt% graphite sample, no extra texturing effect was required to fit the experimental XRD pattern. The heat capacity *Cp* measurement was carried out in the temperature range of 2–300 K on Physical Property Measurement System (PPMS) (Model: 6000, Quantum Design, USA) with the heat capacity option that employs relaxation calorimetry. Raman spectroscopy measurements were carried out using a custom built micro-Raman setup [41] employing 532 nm laser as excitation. Samples were mounted in a liquid nitrogen flow cryostat (Linkam make) and the spectra were recorded in the temperature range 80–300 K in backscattering geometry. The details of Raman Spectroscopic measurements can be obtained elsewhere [42].

3. Results and discussion

Phase purity of the synthesized Sb_2Te_3+x wt% Graphite (x = 0, 0.5) samples is confirmed through X-ray diffraction (XRD). The synchrotron powder diffraction data reveal that both synthesized samples are single phase in nature without presence of impurity phases, at least within the detectable limit of XRD (See Fig. SM1 in supplementary material). No additional peak due to graphite is observed in the XRD data of nanostructured Sb_2Te_3/graphite composite samples. Furthermore, the XRD data indicate a lack of peak shift due to the addition of graphite, which confirms the solid state insolubility of graphite phase in Sb_2Te_3 [21,36]. Thus it can be assumed that graphite is present as separate phase in the present Sb_2Te_3/graphite composite sample. In order to confirm the existence of graphite in x = 0.5 sample, Raman spectroscopic study of both samples (x = 0, 0.5) are carried out (See Fig. SM2 in supplementary material). It is revealed that Raman active vibrational modes of Sb_2Te_3, *i.e*, A_{1g}^1 (~65 cm^{-1}),E_g^2 (~119 cm^{-1}) and A_{1g}^2 (~161 cm^{-1}) are present in both samples, where E_g and A_{1g} modes represent in plane and out of plane vibration respectively (Fig. SM2) [43,44]. The peak around 139 cm^{-1} obtained in both samples can be attributed to the Infra-Red (IR) active mode of Sb_2Te_3. Presence of similar IR active phonon mode in Raman spectra has also been evidenced earlier [45]. In addition to the peaks associated with the vibrational modes of Sb_2Te_3 obtained in both samples, the Raman

spectra of x = 0.5 sample exhibits several Raman-active vibrational modes arising due to graphite. The Raman active modes around 1350, 1580 and 1620 cm^{-1}, as depicted in Fig. SM2 arise due to graphite and can be indexed as D, G and D′ band of graphite, respectively [46]. It is noteworthy to mention that G band, signature of sp^2-hybridized carbon, is one of the most distinct features in Raman spectra of graphitic materials. D, D′ band correspond to defect and disorder induced or edge areas of graphite and is generally absent in highly crystalline graphite. In addition, Raman active peak associated with D + G combination mode (2950 cm^{-1}) is also induced by disorder and is a signature of nanostructured graphite. The peak observed at 2700 cm^{-1} arises due to the overtone of D band (2D) of graphite [47]. Thus Raman spectroscopic measurement along with synchrotron XRD data confirm that graphite is present as separate phases in x = 0.5 sample and has not entered the unit cell of Sb_2Te_3.

In order to investigate the role of graphite addition on κ in Sb_2Te_3, κ(T) measurement of the synthesized Sb_2Te_3/graphite composites is performed and presented in Fig. 1(a). The measured κ value (~1.5 W $m^{-1}K^{-1}$) of pristine Sb_2Te_3 at room temperature is in excellent agreement with the earlier reported data [19]. Temperature dependence of κ_L, κ_L(T) of both samples are also provided in Fig. 1(b). The details of κ_L(T) estimation is provided in the supplementary material [Fig. SM3]. Estimation reveals that κ_e contributes only around 10% of total κ, whereas κ_L dominates κ value, contributing around 90% of total κ for the synthesized samples. Fig. 1(a) and (b) clearly depict that both κ and κ_L values of pristine Sb_2Te_3 decrease by around 40% with graphite addition over the whole temperature range and a low κ_L value of 0.8 W $m^{-1}K^{-1}$ at room temperature is obtained in Sb_2Te_3/graphite nanocomposite sample. The theoretical minimum κ, κ_{min} for Sb_2Te_3 and related nanocomposites can be estimated using the Cahill-Pohl model [48–50]:

$$\kappa_{min} = \frac{1}{2.48} n^{2/3} k_B (v_L + 2v_T) \quad (1)$$

where n,v_L, and v_T represent the number density of the atoms, longitudinal and transverse sound velocities, respectively [14,30]. The low κ_L value, experimentally obtained for x = 0.5 sample, suggests that graphite incorporation helps to approach estimated κ_{min} (~0.31 W $m^{-1}K^{-1}$) of Sb_2Te_3 based nanocomposites.

Thermal variation of specific heat, $C_p(T)$ of Sb_2Te_3 + x wt% graphite (x = 0, 0.5) samples are plotted in Fig. 2. In the temperature range between 200 and 300 K, linear deviation of measured $C_p(T)$ from the Dulong-Petit value, 124.5 J $mol^{-1}K^{-1}$ is observed. The deviation between the measured $C_p(T)$ and theoretical value of specific heat at constant volume C_v ($\Delta C_p = C_p - C_v$) increases with graphite addition. ΔC_p per unit K (ΔC_p/K) changes from 0.015 ± 0.002 J $mol^{-1}K^{-2}$ for x = 0 to 0.096 ± 0.010 J $mol^{-1}K^{-2}$ for x = 0.5 at 300 K. Estimated ΔC_p/K value is of similar order reported earlier for Sb_2Te_3 based system [30]. It is noteworthy to mention that for pristine Sb_2Te_3, ΔC_p/K value does not deviate significantly from the Dulong-Petit value but increases substantially with graphite (x = 0.5) incorporation. Such deviation in $C_p(T)$ data (ΔC_p/K) is a measure of phonon anharmonicity in the system [14,30]. It is reported that phonon anharmonicity helps to scatter phonons and further corroborates with our experimental observation of lower κ (and κ_L) in x = 0.5 sample. A simple fitting of the observed $C_p(T)$ data with Debye model, which accounts for the collective motion of phonons, has also been attempted [14,51]:

$$C_p = \gamma T + 9R\left(\frac{T}{\theta_D}\right)^3 \int_0^{\frac{\theta_D}{T}} \frac{x^4 e^x}{(e^x - 1)^2} dx \quad (2)$$

where γT represents electronic contribution, γ is the Sommerfeld coefficient, and $x = h\nu/k_BT$, $\theta_D = h\nu_D/k_B$, with θ_D is the Debye temperature, ν_D is the Debye frequency, and R is the gas constant. The best fit values of θ_D (~160 K), as obtained from the fitting (Solid lines, Fig. 2), agree fairly well with those reported in literature for Sb_2Te_3 based system [14,52]. However, the Debye model (Eq. (2)), fails to adequately reproduce the experimental data in the low temperature regime (2 K ≤ T ≤ 30 K). The C_p/T^3 vs. T plot (Inset in Fig. 2) of the samples reveals clear deviation from the Debye model below 30 K. The experimental C_p/T^3 vs. T curve for both the samples

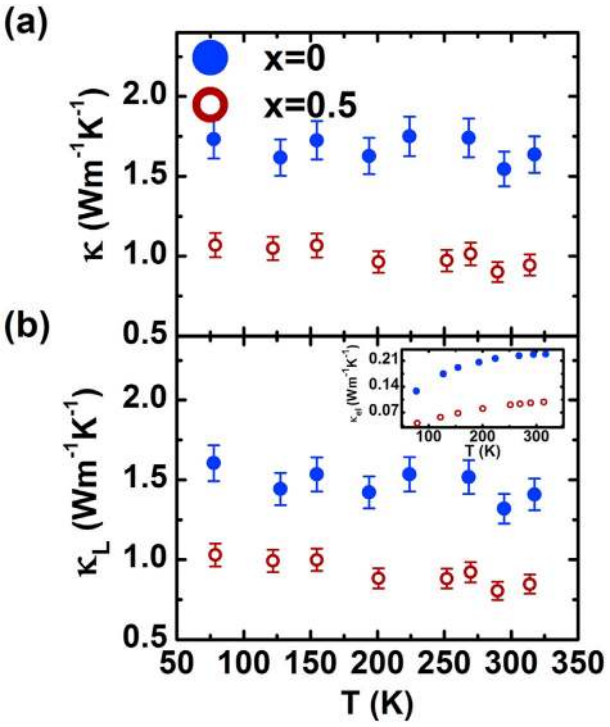

Fig. 1. (Color online) Thermal variation of (a) total thermal conductivity (κ) and (b) lattice thermal conductivity (κ_L) [Inset: electronic part of κ (κ_{el})] for Sb_2Te_3/graphite composite samples.

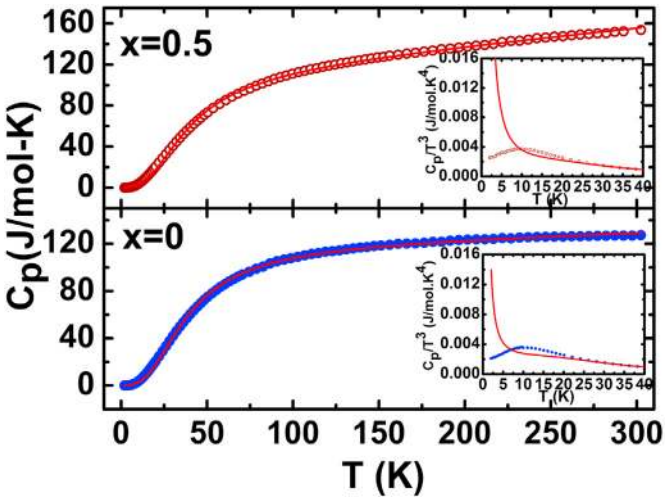

Fig. 2. (Color online) Specific heat at constant pressure (C_p) measured in the range 2–300 K and best fit (red line) to Debye model (Eq. (2)). Inset: C_p/T^3 vs. T plot clearly reveals deviation from the Debye model for T < 30 K.

depicts a broad peak around 10 K, which Debye model fails to reproduce [Fig. 3(c) and (d)]. Also C_p/T vs. T^2 plot shows non-linear nature for both the samples [Fig. 3(a) and (b)]. Attempts have been made earlier to explain this deviation with the help of Schottky model [14,30,53]. But close observation divulges that Schottky model alone cannot explain the deviation observed in the low temperature $C_p(T)$ data ($T \leq 30$ K) and till date the issue has not been resolved fully. To explain this anomaly, the low temperature $C_p(T)$ data (2 K $\leq T \leq$ 30 K) has been interpreted using a two-level Schottky model superimposed to Debye model with embedded Einstein oscillators [54–56]:

$$\frac{C_p}{T} = \gamma + \beta T^2 + \frac{C_S}{T}\left(\frac{\theta_S}{T}\right)^2 \frac{\exp\left(\frac{\theta_S}{T}\right)}{\left[1+\exp\left(\frac{\theta_S}{T}\right)\right]^2} + \sum_n \left(A_n \left(\Theta_{E_n}\right)^2 . \left(T^2\right)^{-\frac{3}{2}} . \frac{\exp\frac{\Theta_{E_n}}{T}}{\left(\exp\frac{\Theta_{E_n}}{T}-1\right)^2} \right) \quad (3)$$

with $\beta = C.\frac{12\pi^4 N_A k_B}{5\theta_D^3}$ and $C = 1 - \sum_n \frac{A_n}{3NR}$

where N_A, C_S, θ_S, A_n, θ_{E_n} and N are Avogadro number, Schottky heat capacity prefactor, Schottky temperature, prefactor of n^{th} Einstein oscillator mode, characteristics temperature of nth Einstein oscillator and number of atoms per formula unit, respectively. Whilst the first term (γ) and second term (βT^2) accounts for the electronic contribution and Debye lattice contribution to C_p, the third term represents Schottky contribution and the fourth term denotes the contribution from Einstein oscillator modes [30,55]. The best fit curves (solid lines) demonstrated in Fig. 3, depict the nice fitting of the experimentally obtained C_p/T vs. T^2 and C_p/T^3 vs. T curve for both the samples. It is observed that 3 Einstein modes are required to satisfactorily model the $C_p(T)$ data. The characteristics temperatures of the respective Einstein modes (θ_{E_1}, θ_{E_2}, θ_{E_3}) and other fitting parameters including θ_S are listed in Table 1. The obtained best fit value of θ_S is in excellent agreement with the literature data [30]. The θ_E values as obtained from the fitting also match fairly well with those reported earlier for Sb_2Te_3 (59 K) [30], Bi_2Te_3 (50 K) [30] and $TlInTe_2$ (25 K, 45 K and 80 K) [55], where the authors interpreted the $C_p(T)$ data by considering combined Debye-Einstein model. However, the present formalism of Einstein oscillators embedded in a Debye host superimposed with Schottky contribution has not been explicitly applied to model the $C_p(T)$ data of Sb_2Te_3 based system. The broad peak observed in the low temperature regime (~10 K) of $C_p(T)$ data for both the samples can be ascribed to the excess phonon density of states (PDOS) resulting from low-lying optical phonon modes [57]. Sb_2Te_3 exhibits layered structure with each layer comprising of quintuple [Te(I)–Sb–Te(II) –Sb–Te(I)] stacks (QLs), where each QL is connected by weak van der Waals force [14]. The quasi-localized low energy optical phonon modes, which arise from these weakly bound atoms are manifested as Einstein oscillators and results in excess contribution to C_p in the low temperature region [55,57]. These low energy optical phonons play an effective role in scattering heat carrying acoustic modes and hinder the thermal transport in the system. So the presence of Einstein oscillator modes is favorable to achieve low κ_L in the present Sb_2Te_3 system. Close observation further reveals that the position of the broad peak (~10 K) in the low-T $C_p(T)$ data does not significantly alter with graphite addition. It can thus be commented that graphite addition has very little influence on the modes of

Table 1
Best fit parameters of C_p/T^3 vs. T plot with Eq. (3): Sommerfeld coefficient γ, prefactor for Debye lattice contribution to $C_p\beta$, Schottky temperature θ_s and Einstein temperatures θ_{E_1},θ_{E_2} and θ_{E_3}.

x	γ(J mol^{-1}K^{-2})	β (J mol^{-1}K^{-4})	θ_s (K)	θ_{E_1}(K)	θ_{E_2}(K)	θ_{E_3}(K)
0	29.3×10^{-4}	6.7×10^{-4}	28	80	47	15
0.5	4.7×10^{-4}	8.5×10^{-4}	27	65	38	11

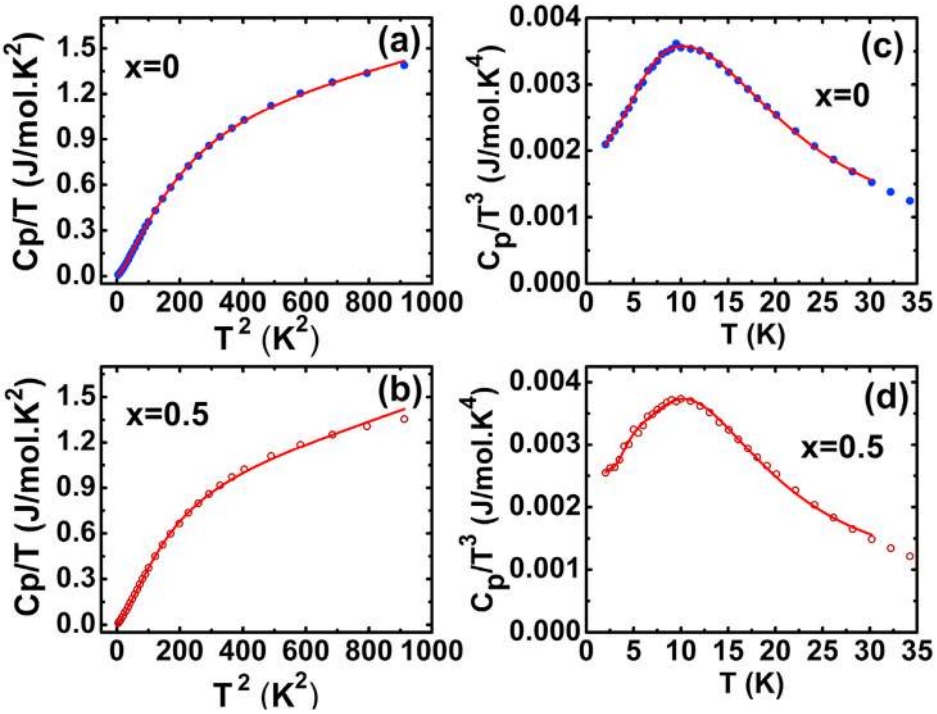

Fig. 3. (Color online) (a), (b) C_p/T vs. T^2 plot and (c), (d) C_p/T^3 vs. T plot for x = 0, 0.5 respectively for 2 K $\leq T \leq$ 30 K. The red lines represent best fit using two-level Schottky model superimposed to a Debye model with embedded Einstein oscillators (Eq. (3)). It is revealed that at least 3 Einstein oscillators are required to fit the data satisfactorily.

Einstein oscillators as well as on dispersion of the low energy optical phonon modes of Sb_2Te_3/graphite composite system. We present a plausible explanation of intrinsic low κ_L observed in Sb_2Te_3 system based on the indepth analysis and modeling $C_p(T)$ data, hitherto unavailable so far.

Attempt has been made to estimate the dislocation density (N_D) macroscopically for both the samples reported here using the temperature dependent synchrotron XRD data. For estimating N_D, modified Williamson-Hall plot was employed, where the broadening of the XRD peaks are strongly related to N_D and crystallite size via

$$\Delta K = \frac{0.9}{d} + \frac{\pi A^2 B_D^2}{2} N_D^{1/2} K^2 C \pm O\left(K^4 C^2\right) \quad (4)$$

The parameter details are provided in the Supplementary materials. From synchrotron powder diffraction the parameters K [$= 2sin\theta_B/\lambda$] and ΔK [$= (\Delta 2\theta_B)cos\theta_B/\lambda$] are calculated, where $\theta_B$is the Bragg angle, $\Delta 2\theta_B$ is the Full Width at Half Maximum (FWHM) of the corresponding diffraction peak at θ_B and λ(= 0.09782 nm) is the wavelength of synchrotron X-ray used. N_D is then obtained from the slope of ΔK vs K^2C curve (C = average dislocation contrast factor). Corresponding plot of the samples for a typical temperature T = 300 K is shown in Fig. 4. From Fig. 5, it can be clearly observed that N_D is higher for x = 0.5 in the whole temperature range of measurement. Presence of graphite dispersoids as second phase at the grain boundary caused lattice mismatch and generate strain between graphite and the unit cell of Sb_2Te_3. This promotes enhancement in N_D for the Sb_2Te_3/graphite composite *i.e.*, x = 0.5 sample. Similar enhancement in N_D has already been reported for $Bi_2Te_{3-x}Se_x$ and PbTe–PbS TE systems [58,59]. The enhanced dislocations, which are 1D defects, scatter mid-frequency phonons through the dislocation cores and strain [8,9,60] and effectively reduce κ_L in x = 0.5 sample. In addition, presence of graphite in the grain boundary regime increases the number of Sb_2Te_3/graphite 2D heterointerfaces, which helps to scatter low frequency phonons [19,21]. In accordance to the recent report of Jin et al., it may be emphasized that to engineer an effective heterointerface optimum size of Sb_2Te_3 nanocrystals is ~10 nm thickness with uniform hexagonal morphology [61]. Furthermore, graphite also acts as point defects (0D) and significantly contributes in scattering high frequency phonons in x = 0.5 sample. Our comprehensive analysis suggests that graphite addition plays a pivotal role in scattering low, mid and high frequency phonons by developing effective 2D (heterointerfaces), 1D (enhanced dislocations) and 0D (point defects) scattering sources in Sb_2Te_3/graphite composite sample, thereby lowering κ_L.

Temperature dependent synchrotron powder XRD of both of the

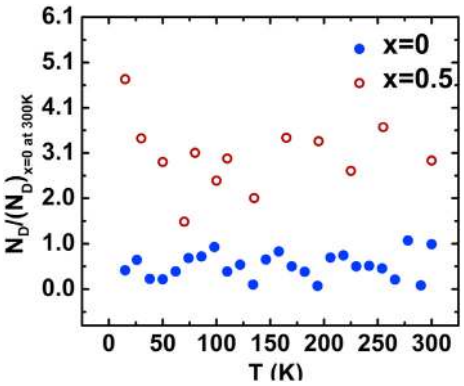

Fig. 5. (Color online) Temperature dependence of ratio of dislocation density (N_D) for the samples calculated using modified Williamson-Hall plot.

Sb_2Te_3 + x wt% graphite (x = 0, 0.5) was performed in the temperature range 15 K ≤ T ≤ 300 K. The samples retain rhombohedral crystal structure (space group $R\bar{3}m$), with A_7-type rhombohedral phase until lowest temperature of measurement (T = 15 K). The diffraction patterns obtained after Rietveld refinement are presented in Supplemental Material. Thermal variation of structural parameters, *i.e.*, *a* and *c* of x = 0 and 0.5 samples, extracted using Rietveld refinement, is also provided in the supplementary material (Fig. SM4). The refined lattice parameters, *i.e.*, *a* and *c* increase monotonically with increasing temperature, indicating usual positive thermal expansion coefficients in both orientations for the synthesized samples. Thermal expansion coefficient is an important parameter, not only for device designing, but also the strain induced due to change in temperature may affect its phonon dynamics [14,30,43,51,62]. So, attempt has been made to study the thermal expansion coefficient in details and explore the corresponding physics towards obtaining better insight about phonon dynamics of the synthesized Sb_2Te_3/graphite composite samples. The linear thermal expansion coefficients$\alpha_L$are obtained from the derivative, $\alpha_L = \frac{d(\ln L)}{dT}$, of the lattice constants, where *L* denotes lattice constants *a* and *c*. The extracted $\alpha_L$values are in excellent agreement with the previously reported thermal expansivity data [51,52]. These data appear to be more scattered beyond ~150 K, this anomalous behavior being more pronounced for the x = 0 sample. The obtained$\alpha_L(T)$data is fitted with the Debye model [14,43,51]:

$$\alpha_L(T) = \alpha_0 \left(\frac{T}{\theta_D}\right)^3 \int_0^{\frac{\theta_D}{T}} \frac{x^4 e^x}{(e^x - 1)^2} dx \quad (5)$$

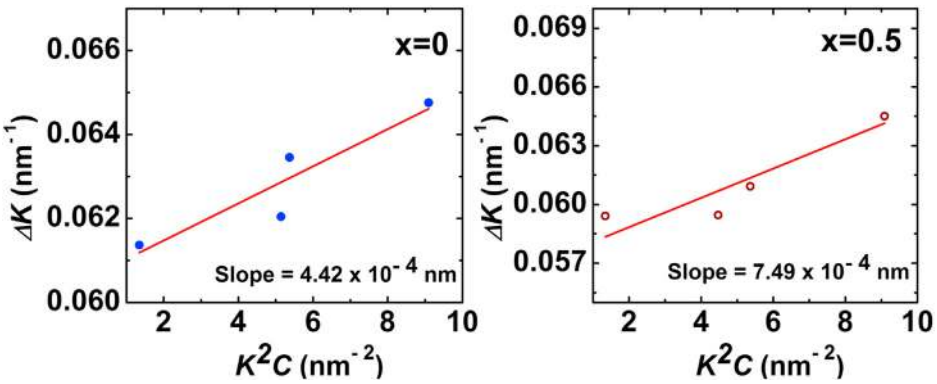

Fig. 4. (Color online) Modified Williamson–Hall plot from synchrotron XRD pattern analysis at a typical temperature T = 300 K for the samples indicating larger slope for x = 0.5 as compared to x = 0.

where α_0 is a constant and θ_D is the Debye Temperature. $\theta_D = 160$ K, as obtained from the fitting of $C_p(T)$ data with Debye model, is used for fitting the $\alpha_L(T)$data. Solid lines in Fig. 6 represent the best fit obtained using Debye model. Fig. 6 clearly depicts that below θ_D both α_a and $\alpha_c$are well fitted by this model. In contrast, above θ_D both the agreement is less obvious as the α_a and $\alpha_c$experimental values are more scattered. Such deviation of $\alpha_L$from the Debye model, reported earlier for Sb_2Te_3 related systems, has generally been ascribed to the presence of higher order anharmonic effect in the system [63]. Anomalous behavior of van der Waals forces between Quintuple layers (QL) of Sb_2Te_3 at high temperature could also be a reason for the observed deviation [52]. But departure of both $\alpha_a$and $\alpha_c$from Debye model above θ_D consolidates the idea that phonon anharmonicity prevails in the synthesized Sb_2Te_3 based samples discussed here. It is noteworthy to mention that anharmonic lattice vibrations help to reduce κ_L by scattering phonons of all frequency and explains the low κ_L values observed in Sb_2Te_3 based system. However, the role of graphite addition on lattice anharmonicity has been investigated further in order to address the observed 40% reduction of κ_L for x = 0.5 sample.

To confirm phonon anharmonicity in Sb_2Te_3/graphite nanocomposite samples, in-depth temperature dependent Raman spectroscopic study in the range from 300 K to 80 K is carried out. No additional Raman mode other than those appeared at 300 K (discussed above) is observed down to 80 K for both samples. The Raman spectra of both the samples are fitted with Lorentzian function and the extracted temperature dependence of phonon frequency (peak positions, ω) are used for analysis of lattice anharmonicity. Temperature dependent phonon frequency of all the characteristics phonon modes of Sb_2Te_3 *i.e.*, A_{1g}^1 ,E_g^2 and A_{1g}^2, as obtained for both synthesized samples, are plotted in Fig. 7. The phonon frequencies for all the phonon modes soften and broaden with increase of temperature. Such temperature induced hardening and softening have been reported earlier for different materials including Bi_2Te_3, Bi_2Se_3, Sb_2Te_3 [14,43,62] and indicate the anharmonic nature of the characteristic phonon modes. The observed temperature dependence of phonon frequency and departure from its bare harmonic value owe mostly to the phonon-phonon coupling in the system. This phonon-phonon coupling renormalizes the phonon energy and lifetime and we get non-zero higher (>2nd) order anharmonic terms from the polynomial expansion of the lattice potential in normal coordinates. To quantify the anharmonic part arising due to phonon-phonon coupling, the simplest approximation is to use symmetrical three phonon coupling model, also known as Klemens's model [43,64,65]. This model works based on the assumption that an optical phonon decays into two phonons with equal energies and opposite momentum. The model does not take into account the "coalescence" process where two phonons fuse into a third phonon [66]. While this model is successful in describing thermal variation of phonon in some materials [67], more general approach is to use an approximation which also includes anharmonic contributions due to thermal expansion and asymmetric decay into two or more different phonons [68–70]. According to the generalized Klemens's model, the temperature dependence of phonon frequency can be expressed as:

$$\omega(T) = \omega_0 + \Delta\omega^{(1)}(T) + \Delta\omega^{(2)}(T) \tag{6}$$

where ω_0 is bare harmonic frequency; $\Delta\omega^{(1)}(T)$is the anharmonic correction arising due to the lattice thermal expansion originating from the thermal expansion induced changes in the harmonic force constant. The term $\Delta\omega^{(1)}(T)$ is described as:

$$\Delta\omega^{(1)}(T) = \omega_0\left[\exp\left(-\gamma_G\int_0^T[\alpha_c(T') + 2\alpha_a(T')]dT'\right) - 1\right] \tag{7}$$

where γ_G is the Grüneisen parameter [14,51]. $\Delta\omega^{(2)}(T)$ is anharmonic phonon-phonon coupling term and is represented by:

$$\Delta\omega^{(2)}(T) = A_1[1 + n(\omega_1) + n(\omega_2)] \tag{8}$$

with $\omega_1 = \omega_2 = \omega_0/2$ and$n(\omega) = [\exp(h\omega/k_BT) - 1]^{-1}$; where '$A_1$' is the fitting parameter.

The best theoretical fit to Klemens's model (Eq. (6)) for the Raman activeA_{1g}^1 ,E_g^2 and A_{1g}^2phonon modes of both x = 0 and 0.5 samples is represented by individual solid lines in Fig. 7. The obtained best fit values of bare harmonic frequency, ω_0, for all the characteristics phonon modes are presented in Table 2. It is observed that ω_0 for all the phonon modes increases with graphite addition. At room temperature and 1 atm pressure, pressure coefficients for A_{1g}^1 ,E_g^2 and A_{1g}^2phonon modes are 4.30, 2.11, 2.57 cm^{-1} GPa^{-1}, respectively [71]. From the observed shift of ω_0(Table 2), it is further revealed that in x = 0.5 sample, graphite provides a large compressive strain to the Sb_2Te_3 matrix [72]. Such strain on the matrix due to graphite incorporation creates dislocation in Sb_2Te_3 [73,74] and corroborates with the XRD analysis which confirms higher dislocation density (N_D) in the x = 0.5

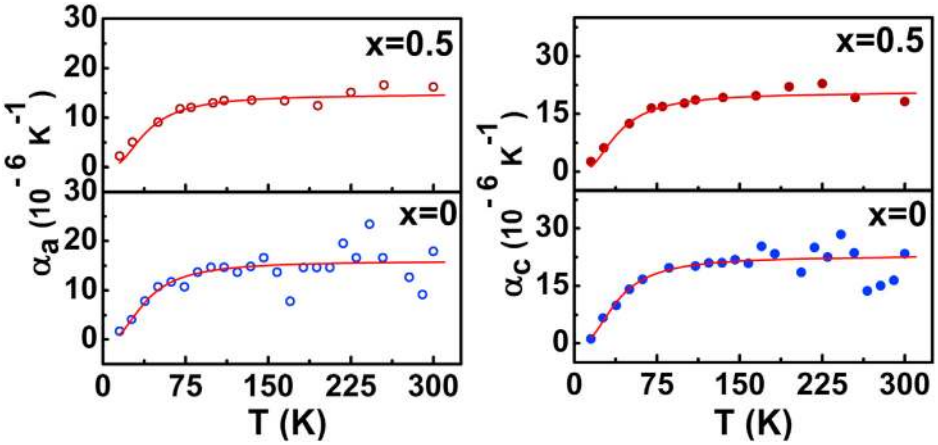

Fig. 6. (Color online) Temperature dependent linear thermal expansion coeffecient α_Li.e., α_a and $\alpha_c$for x = 0 and x = 0.5. The errors in α_a and $\alpha_c$are within the size of the data points. Red lines show attempted fitting with Debye model.

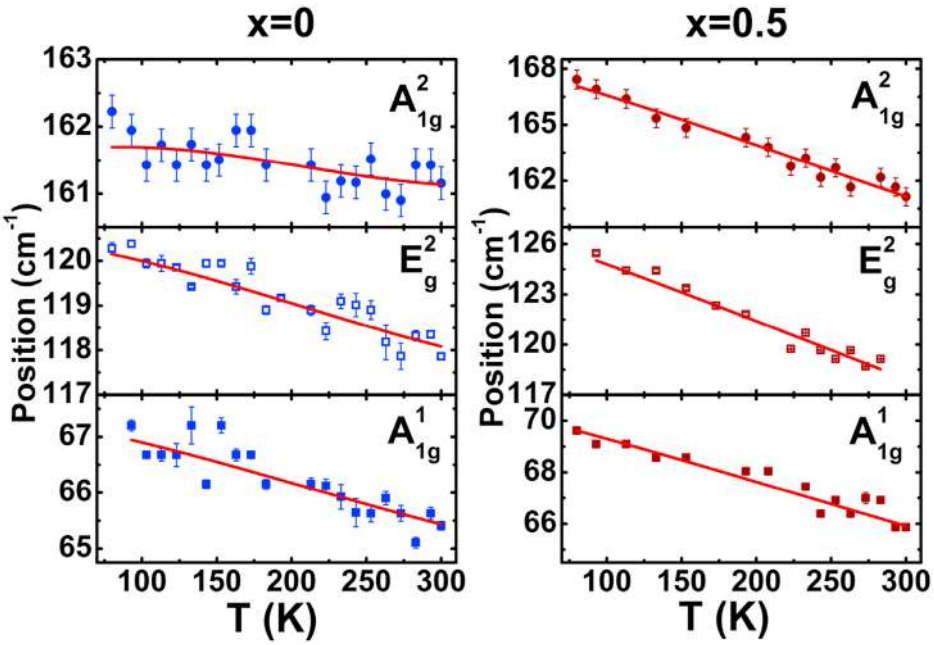

Fig. 7. (Color online) Temperature dependence of the phonon frequency for Sb_2Te_3 + x wt% graphite samples showing softening of all modes with increasing temperature. The data has been fitted with Klemens's model (Eq. (6)) to investigate phonon anharmonicity in the samples.

Table 2
Bare harmonic frequency, ω_0 of all the characteristics phonon modes A^1_{1g},E^2_g and A^2_{1g} for x = 0 and 0.5 extracted from fitting temperature dependence of phonon frequency with Eq. (6) and additional pressure exerted on Sb_2Te_3 matrix due to addition of graphite in x = 0.5 sample.

Raman Mode	ω_0 for x = 0 (cm^{-1})	ω_0 for x = 0.5 (cm^{-1})	Net pressure due to graphite addition (GPa)
A^1_{1g}	67.39	70.79	0.75
E^2_g	120.53	127.86	2.04
A^2_{1g}	161.40	168.82	2.47

sample. The interfaces between the graphite and main Sb_2Te_3 phase in Sb_2Te_3/graphite nanocomposite thus introduces lattice strain in the system and plays a beneficial role to the suppression of κ_L [72].

To gain further quantitative insights, we focus on the temperature dependence part of phonon frequency (Eq. (6)). As mentioned above, the anharmonic contribution to phonon vibration comes from two sources: $\Delta\omega(T) = \Delta\omega^{(1)}(T) + \Delta\omega^{(2)}(T)$. Temperature dependence of $\Delta\omega^{(1)}(T)$ and $\Delta\omega^{(2)}(T)$ of all the three characteristics phonon modes A^1_{1g} ,E^2_g and A^2_{1g} are calculated individually using Eqs. (7) and (8) for both samples and plotted in Fig. 8. Fig. 8(a) reveals that $|\Delta\omega^{(1)}(T)|$ is higher in x = 0 sample, *i.e.*, anharmonic contribution from lattice thermal expansion is larger in the pristine sample. The estimated large compressive strain in Sb_2Te_3 matrix affects its harmonic force constant and is reflected in the observed lower anharmonicity of lattice thermal expansion of Sb_2Te_3/graphite composite (x = 0.5) sample. The temperature dependent variation of $|\Delta\omega^{(1)}(T) + \Delta\omega^{(2)}(T)|$ for all the characteristics phonon modes of Sb_2Te_3 are plotted in Fig. 9. It is clearly revealed that the phonon-phonon coupling term $|\Delta\omega^{(2)}(T)|$is much higher in x = 0.5 sample (Fig. 8(b)). Furthermore, changes in $|\Delta\omega^{(2)}(T)|$overwhelms$|\Delta\omega^{(1)}(T)|$, such that the overall anharmonic contribution to phonon vibration, *i.e.*, $|\Delta\omega^{(1)}(T) + \Delta\omega^{(2)}(T)|$becomes larger in x = 0.5 sample (Fig. 9). This high $|\Delta\omega^{(2)}(T)|$ in Sb_2Te_3/graphite nanocomposite indicates that graphite acts as a mediator for phonon-phonon coupling and plays a significant role in enhancing the anharmonic contribution to phonon vibration. This higher phonon anharmonicity in graphite contained composite sample helps in suppressing κ_L by scattering phonons of all frequency.

Strong phonon scattering effect is reported to be also effective in Bi_2Te_3/CNT composite system [16,18,61], where heterointerfaces, nanopores and other defects efficiently suppress thermal transport. Bi_2Te_3/SWCNT (Single wall carbon nanotube) based hybrid sample has recently been reported as an excellent route for the design and fabrication of high-performance flexible TE materials [61]. Our results clearly indicate that nanocompositing with graphite, which is also a carbon-based material, is a favorable route for reducing κ_L keeping Seebeck coefficient unchanged. However, it may be acknowledged that such low 0.5 wt % of graphite giving a small molar ratio (Sb_2Te_3:C = 3.835:1) is already too high to avoid an increase of the grain boundary resistance and as mentioned in our previous report on Sb_2Te_3/graphite nanocomposites, as far as ZT value is concerned the positive effect in κ_L is subdued by decrease in electrical conductivity with graphite addition [36]. It is noteworthy to mention that in Sb_2Te_3/Ag_2Te composite, Lee et al. achieved similar κ_L reduction of 50%, but with 35 wt% of Ag_2Te [34]. In the other report of Sb_2Te_3 based composite with PEDOT [33], the thermoelectric properties of the pristine Sb_2Te_3 (*ZT*~0.15 at 300 K) are much lower than those reported by us [36]. In that respect, the present study showing the graphite potentialities should be completed in the future with lower graphite concentration to avoid such drastic electrical conductivity degradation. The approach of

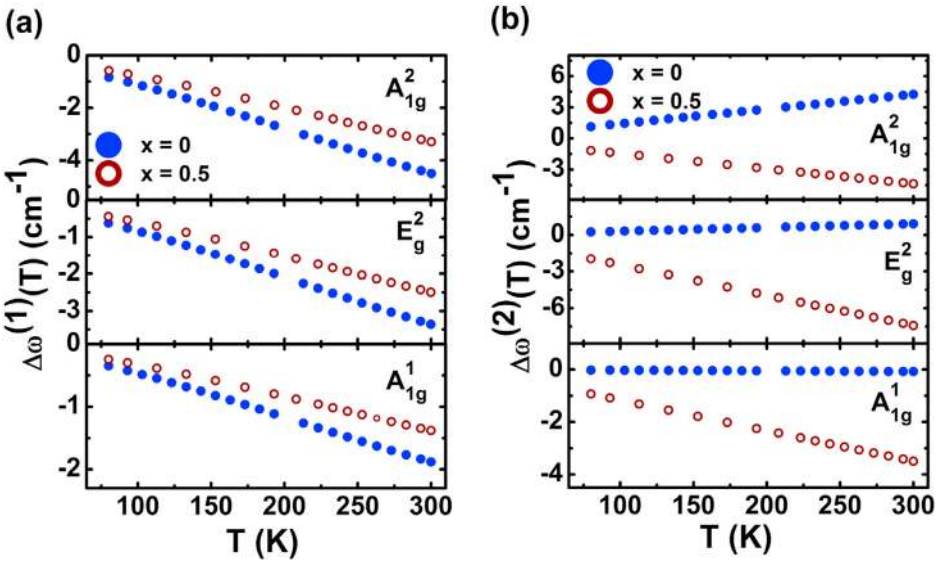

Fig. 8. (Color online) Thermal variation of $\Delta\omega^{(1)}(T)$ and $\Delta\omega^{(2)}(T)$revealing that anharmonic correction arising due to the lattice thermal expansion is greater for pristine sample while phonon-phonon coupling is higher in Sb_2Te_3/graphite nanocomposite.

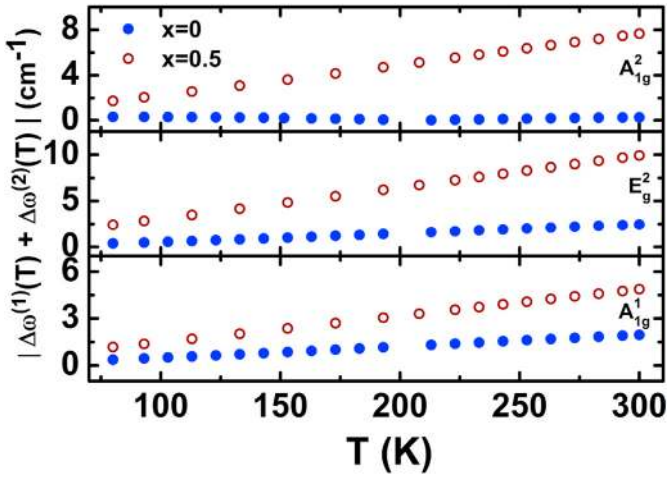

Fig. 9. (Color online) Total anharmonicity present in the samples for the whole temperature range under investigation.

nanocompositing with graphitic materials can be applicable to a series of similar layered TE materials, including Bi_2Te_3, Bi_2Se_3 and Sb_2Te_3, and both *n*- and *p*-type TE materials can be fabricated using this method [61].

4. Conclusion

Advances in TE materials are intimately related to the reduction of κ_L, the only independent parameter in ZT. In this work, the efficiency of graphite on suppressing κ_L in Sb_2Te_3/graphite nanocomposite system is demonstrated. Graphite effectively contributes in scattering phonons of different length scale and intensifies phonons scattering rate. Dispersion of graphite in Sb_2Te_3 also modulates phonon anharmonicity and enhances scattering of phonons over the entire spectrum. The synergistic role of graphite in ~40% reduction of κ_L value observed in nanostructured Sb_2Te_3/graphite composite system makes the present strategy a possible route to improve TE materials. Thus, nanocompositing with graphite is worth trying for lower graphite concentration in Sb_2Te_3 and applying to other TE materials.

Declaration of competing interest

The authors declare that they have no known competing financial interests or personal relationships that could have appeared to influence the work reported in this paper.

Acknowledgments

The authors gratefully acknowledge IUAC, New Delhi, India (Project reference no.:UFR-65307) and UGC DAE CSR, Kolkata, India (Project reference no.: UGC-DAE-CSR-KC/CRS/19/MS02/0939) for providing financial support for carrying out this work. They would also like to thank the Department of Science and Technology, India for financial support during the experiments at the Indian Beamline, Photon Factory, KEK, Japan. Author P. Singha is thankful to UGC DAE CSR, Kolkata Centre, Govt. of India for providing him research fellowship. Author Subarna Das is grateful to UGC, Govt. of India for providing senior research fellowship and also acknowledges the support received through 'Raman-Charpak Fellowship 2019' jointly funded by the Department of Science and Technology (DST), Government of India and the French Institute in India (IFI), French Embassy in India, Ministry for Europe and Foreign Affairs, Government of France.

Appendix A. Supplementary data

Supplementary data to this article can be found online at https://doi.org/10.1016/j.jmat.2020.11.014.

References

[1] Snyder GJ, Toberer ES. Complex thermoelectric materials. Nat Mater 2008;7:105–14. https://doi.org/10.1038/nmat2090.
[2] Pandey T, Lindsay L, Sales BC, Parker DS. Lattice instabilities and phonon thermal transport in TlBr. Phys Rev Mater 2020;4:045403. https://doi.org/10.1103/PhysRevMaterials.4.045403.
[3] Chen Z, Zhang X, Pei Y. Manipulation of phonon transport in thermoelectrics. Adv Mater 2018;30:1705617. https://doi.org/10.1002/adma.201705617.
[4] Du Y, Xu J, Paul B, Eklund P. Flexible thermoelectric materials and devices.

Appl Mater Today 2018;12:366–88. https://doi.org/10.1016/j.apmt.2018.07.004.
[5] Beretta D, Neophytou N, Hodges JM, Kanatzidis MG, Narducci D, Martin-Gonzalez M M, Beekman M, Balke B, Cerretti G, Tremel W, Zevalkink A, Hofmann AI, Muller C, Dorling B, Campoy-Quiles M, Caironi M. Thermoelectrics: from history, a window to the future. Mat Sci Eng R 2019;138:210–55. https://doi.org/10.1016/j.mser.2018.09.001.
[6] Freer R, Powell AV. Realising the potential of thermoelectric technology: a Roadmap. J Mater Chem C 2020;8:441–63. https://doi.org/10.1039/C9TC05710B.
[7] Biswas K, He J, Blum ID, Wu CI, Hogan TP, Seidman DN, Dravid VP, Kanatzidis MG. High-performance bulk thermoelectrics with all-scale hierarchical architectures. Nature 2012;489:414–8. https://doi.org/10.1038/nature11439.
[8] Kim SI, Lee KH, Mun HA, Kim HS, Hwang SW, Roh JW, Yang DJ, Shin WH, Li XS, Lee YH, Snyder GJ, Kim SW. Dense dislocation arrays embedded in grain boundaries for high-performance bulk thermoelectrics. Science 2015;348:109–14. https://doi.org/10.1126/science.aaa4166.
[9] Chen Z, Ge B, Li W, Lin S, Shen J, Chang Y, Hanus R, Snyder GJ, Pei Y. Vacancy-induced dislocations within grains for high-performance PbSe thermoelectrics. Nat Commun 2017;8:13828. https://doi.org/10.1038/ncomms13828.
[10] Maignan A, Daou R, Guilmeau E, Berthebaud D, Barbier T, Lebedev O, Hébert S. Thermoelectric properties, metal-insulator transition, and magnetism: Revisiting the $Ni_{1-x}Cu_xS_2$ system. Phys Rev Mater 2019;3:115401. https://doi.org/10.1103/PhysRevMaterials.3.115401.
[11] Dutta M, Matteppanavar S, Prasad MVD, Pandey J, Warankar A, Mandal P, Soni A, Waghmare UV, Biswas K. Ultralow thermal conductivity in chain-like TlSe due to inherent Tl^+ rattling. J Am Chem Soc 2019;141:20293–9. https://doi.org/10.1021/jacs.9b10551.
[12] Xie W, Tang X, Yan Y, Zhang Q, Tritt TM. Unique nanostructures and enhanced thermoelectric performance of melt-spun BiSbTe alloys. Appl Phys Lett 2009;94:102111. https://doi.org/10.1063/1.3097026.
[13] Lee S, Esfarjani K, Luo T, Zhou J, Tian Z, Chen G. Resonant bonding leads to low lattice thermal conductivity. Nat Commun 2014;5:3525. https://doi.org/10.1038/ncomms4525.
[14] Das D, Das S, Singha P, Malik K, Deb AK, Bhattacharya A, Kulbachinskii VA, Basu R, Dhara S, Bandyopadhyay S, Banerjee A. Evolution of phonon anharmonicity in Se-doped Sb_2Te_3 thermoelectrics. Phys Rev B 2017;96:064116. https://doi.org/10.1103/PhysRevB.96.064116.
[15] Liu Q, Shao R, Li N, Liang W, Yang X, Luo SN, Zhao Y. Anharmonicity of Bi_2Se_3 revealed by fs transient optical spectroscopy. Appl Phys Lett 2019;115:201902. https://doi.org/10.1063/1.5131257.
[16] Kim KT, Choi SY, Shin EH, Moon KS, Koo HY, Lee GG, Ha GH. The influence of CNTs on the thermoelectric properties of a CNT/Bi_2Te_3 composite. Carbon 2013;52:541–9. https://doi.org/10.1016/j.carbon.2012.10.008.
[17] Ibanez M, Luo Z, Genc A, Piveteau L, Ortega S, Cadavid D, Dobrozhan O, Liu Y, Nachtegaal M, Zebarjadi M, Arbiol J, Kovalenko MV, Cabot A. High-performance thermoelectric nanocomposites from nanocrystal building blocks. Nat Commun 2016;7:10766. https://doi.org/10.1038/ncomms10766.
[18] Zhang Q, Xu L, Zhou Z, Wang L, Jiang W, Chen L. Constructing nanoporous carbon nanotubes/Bi_2Te_3 composite for synchronous regulation of the electrical and thermal performances. J Appl Phys 2017;121:055104. https://doi.org/10.1063/1.4975467.
[19] Ahmad M, Agarwal K, Kumari N, Mehta BR. KPFM based investigation on the nature of Sb_2Te_3:MoS_2 and Bi_2Te_3:MoS_2 2D interfaces and its effect on the electrical and thermoelectric properties. Appl Phys Lett 2017;111:023904. https://doi.org/10.1063/1.4991359.
[20] Soni A, Shen Y, Yin M, Zhao Y, Yu L, Hu X, Dong Z, Khor KA, Dresselhaus MS, Xiong Q. Interface driven energy filtering of thermoelectric power in spark plasma sintered $Bi_2Te_{2.7}Se_{0.3}$ nanoplatelet composites. Nano Lett 2012;12:4305–10. https://doi.org/10.1021/nl302017w.
[21] Agarwal K, Kaushik V, Varandani D, Dhar A, Mehta BR. Nanoscale thermoelectric properties of Bi_2Te_3 – graphene nanocomposites: Conducting atomic force, scanning thermal and kelvin probe microscopy studies. J Alloys Compd 2016;681:394–401. https://doi.org/10.1016/j.jallcom.2016.04.161.
[22] Popescu A, Datta A, Nolas GS, Wood LM. Thermoelectric properties of Bi-doped PbTe composites. J Appl Phys 2011;109:103709. https://doi.org/10.1063/1.3586240.
[23] Wang YY, Cai KF, Yin JL, An BJ, Du Y, Yao X. In situ fabrication and thermoelectric properties of PbTe–polyaniline composite nanostructures. J Nanopart Res 2011;13:533–9. https://doi.org/10.1007/s11051-010-0043-y.
[24] Blank VD, Buga SG, Kulbachinskii VA, Kytin VG, Medvedev VV, Popov MY, Stepanov PB, Skok VF. Thermoelectric properties of $Bi_{0.5}Sb_{1.5}Te_3/C_{60}$ nanocomposites. Phys Rev B 2012;86:075426. https://doi.org/10.1103/PhysRevB.86.075426.
[25] Ibanez M, Zamani R, Gorsse S, Fan J, Ortega S, Cadavid D, Morante JR, Arbiol J, Cabot A. Core–shell nanoparticles as building blocks for the bottom-up production of functional nanocomposites: PbTe–PbS thermoelectric properties. ACS Nano 2013;7:2573–86. https://doi.org/10.1021/nn305971v.
[26] Tan G, Shi F, Sun H, Zhao LD, Uher C, Dravid VP, Kanatzidis MG. SnTe–$AgBiTe_2$ as an efficient thermoelectric material with low thermal conductivity. J Mater Chem A 2014;2:20849–54. https://doi.org/10.1039/C4TA05530F.
[27] Guo H, Xin H, Qin X, Jian Z, Li D, Li Y, Li C. Thermoelectric transport properties of PbTe-based composites incorporated with Cu_2Se nano-inclusions. J Phys D Appl Phys 2016;49:065302. https://doi.org/10.1088/0022-3727/49/6/065302.
[28] Guo H, Xin H, Qin X, Zhang J, Li D, Li Y, Song C, Li C. Enhanced thermoelectric performance of highly oriented polycrystalline SnSe based composites incorporated with SnTe nanoinclusions. J Alloys Compd 2016;689:87–93. https://doi.org/10.1016/j.jallcom.2016.07.291.
[29] He J, Xu J, Tan X, Liu GQ, Shao H, Liu Z, Jiang H, Jiang J. Synthesis of SnTe/$AgSbSe_2$ nanocomposite as a promising lead-free thermoelectric material. J Materiomics 2016;2:165–71. https://doi.org/10.1016/j.jmat.2016.05.001.
[30] Bessas D, Sergueev I, Wille HC, Perßon J, Ebling D, Hermann RP. Lattice dynamics in Bi_2Te_3 and Sb_2Te_3: Te and Sb density of phonon states. Phys Rev B 2012;86:224301. https://doi.org/10.1103/PhysRevB.86.224301.
[31] Das D, Malik K, Deb AK, Dhara S, Bandyopadhyay S, Banerjee A. Defect induced structural and thermoelectric properties of Sb_2Te_3 alloy. J Appl Phys 2015;118:045102. https://doi.org/10.1063/1.4927283.
[32] Rieger F, Roddatis V, Kaiser K, Bendt G, Schulz S, Jooss C. Transition into a phonon glass in crystalline thermoelectric $(Sb_{1-x}Bi_x)_2Te_3$ films. Phys Rev Mater 2020;4:025402. https://doi.org/10.1103/PhysRevMaterials.4.025402.
[33] Zheng W, Bi P, Kang H, Wei W, Liu F, Shi J, Peng L, Wang Z, Xiong R. Low thermal conductivity and high thermoelectric figure of merit in p-type Sb_2Te_3/poly(3,4-ethylenedioxythiophene) thermoelectric composites. Appl Phys Lett 2014;105:023901. https://doi.org/10.1063/1.4887504.
[34] Lee MH, Kim KR, Rhyee JS, Park SD, Snyder GJ. High thermoelectric figure-of-merit in Sb_2Te_3/Ag_2Te bulk composites as Pb-free p-type thermoelectric materials. J Mater Chem C 2015;3:10494–9. https://doi.org/10.1039/C5TC01623A.
[35] Pierson HO. Handbook of carbon, graphite, diamond and fullerenes: properties, processing and applications (noyes publications, park ridge, NJ, 1994). Chung DDL. J Mater Sci 2002;37:1475.
[36] Das S, Singha P, Deb AK, Das SC, Chatterjee S, Kulbachinskii VA, Kytin VG, Zinoviev DA, Maslov NV, Dhara S, Bandyopadhyay S, Banerjee A. Role of graphite on the thermoelectric performance of Sb_2Te_3/graphite nanocomposite. J Appl Phys 2019;125:195105. https://doi.org/10.1063/1.5095935.
[37] Zaikina JV, Kovnir KA, Sobolev AN, Presniakov IA, Kytin VG, Kulbachinskii VA, Olenev AV, Lebedev OI, Tendeloo GV, Dikarev EV, Shevelkov AV. Highly disordered crystal structure and thermoelectric properties of Sn_3P_4. Chem Mater 2008;20:2476–83. https://doi.org/10.1021/cm702655g.
[38] Van Berkum JGM, Sprong GJM, Keijser T, Delhez R, Sonneveld EJ. The optimum standard specimen for X-ray diffraction line-profile analysis. Powder Diffr 1995;10:129–39. https://doi.org/10.1017/S0885715600014512.
[39] Lutterotti L, Matthies S, Wenk HR. In: Spunar JA, editor. Proceeding of ICOTOM14. Ottawa: National Research Council of Canada; 1999. p. 1599. IUCr: Newsl. CPD 1999; 21: 14.
[40] Popa NC. The (*hkl*) dependence of diffraction-line broadening caused by strain and size for all laue groups in Rietveld refinement. J Appl Cryst 1998;31:176–80. https://doi.org/10.1107/S0021889897009795.
[41] Kumar GVP, Narayana C. Adapting a fluorescence microscope to perform surface enhanced Raman spectroscopy. Curr Sci 2007;93:778–81.
[42] Barman N, Singh P, Narayana C, Varma KBR. Incipient ferroelectric to a possible ferroelectric transition in Te^{4+} doped calcium copper titanate ($CaCu_3Ti_4O_{12}$) ceramics at low temperature as evidenced by Raman and dielectric spectroscopy. AIP Adv 2017;7:035105. https://doi.org/10.1063/1.4973645.
[43] Kim Y, Chen X, Wang Z, Shi J, Miotkowski I, Chen YP, Sharma PA, Sharma ALL, Hekmaty MA, Jiang Z, Smirnov D. Temperature dependence of Raman-active optical phonons in Bi_2Se_3 and Sb_2Te_3. Appl Phys Lett 2012;100:071907. https://doi.org/10.1063/1.3685465.
[44] Das D, Malik K, Deb AK, Kulbachinskii VA, Kytin VG, Chatterjee S, Das D, Dhara S, Bandyopadhyay S, Banerjee A. Tuning of thermoelectric properties with changing Se content in Sb_2Te_3. Europhys Lett 2016;113:47004. https://doi.org/10.1209/0295-5075/113/47004.
[45] Zheng B, Sun Y, Wu J, Han M, Wu X, Huang K, Feng S. Group IV semiconductor Ge integration with topological insulator Sb_2Te_3 for spintronic application. J Phys D Appl Phys 2017;50:105303. https://doi.org/10.1088/1361-6463/aa57a0.
[46] Saito R, Hofmann M, Dresselhaus G, Jorio A, Dresselhaus MS. Raman spectroscopy of graphene and carbon nanotubes. Adv Phys 2011;60:413–550. https://doi.org/10.1080/00018732.2011.582251.
[47] Pimenta MA, Dresselhaus G, Dresselhaus MS, Cancado LG, Jorio A, Saito R. Studying disorder in graphite-based systems by Raman spectroscopy. Phys Chem Chem Phys 2007;9:1276–90. https://doi.org/10.1039/B613962K.
[48] Cahill DG, Pohl RO. Lattice vibrations and heat transport in crystals and glasses. Annu Rev Phys Chem 1988;39:93–121. https://doi.org/10.1146/annurev.pc.39.100188.000521.
[49] Chen W, Pöhls JH, Hautier G, Broberg D, Bajaj S, Aydemir U, Gibbs ZM, Zhu H, Asta M, Snyder GJ, Meredig B, White MA, Persson K, Jain A. Understanding thermoelectric properties from high-throughput calculations: trends, insights, and comparisons with experiment. J Mater Chem C 2016;4:4414–26. https://doi.org/10.1039/C5TC04339E.
[50] Wei P, Yang J, Guo L, Wang S, Wu L, Xu X, Zhao W, Zhang Q, Zhang W, Dresselhaus MS, Yang J. Minimum thermal conductivity in weak topological insulators with Bismuth-based stack structure. Adv Funct Mater 2016;26:5360–7. https://doi.org/10.1002/adfm.201600718.
[51] Das D, Malik K, Das S, Singha P, Deb AK, Kulbachinskii VA, Basu R, Dhara S, Dasgupta A, Bandyopadhyay S, Banerjee A. Modulation of thermal conductivity and thermoelectric figure of merit by anharmonic lattice vibration in Sb_2Te_3 thermoelectrics. AIP Adv 2018;8:125119. https://doi.org/10.1063/

1.5053174.
[52] Dutta P, Bhoi D, Midya A, Khan N, Mandal P, Samatham SS, Ganesan V. Anomalous thermal expansion of Sb_2Te_3 topological insulator. Appl Phys Lett 2012;100:251912. https://doi.org/10.1063/1.4730390.
[53] Saint-Paul M, Lasjaunias JC, Locatelli M. Low-temperature thermal properties of neutron-irradiated crystalline quartz. J Phys C 1982;15:2375. https://doi.org/10.1088/0022-3719/15/11/018.
[54] Liu H, Yang J, Shi X, Danilkin SA, Yu D, Wang C, Zhang W, Chen L. Reduction of thermal conductivity by low energy multi-Einstein optic modes. J Materiomics 2016;2:187–95. https://doi.org/10.1016/j.jmat.2016.05.006.
[55] Jana MK, Pal K, Warankar A, Mandal P, Waghmare UV, Biswas K. Intrinsic rattler-induced low thermal conductivity in Zintl type $TlInTe_2$. J Am Chem Soc 2017;139:4350–3. https://doi.org/10.1021/jacs.7b01434.
[56] Xie H, Su X, Hao S, Wolverton C, Uher C, Tang X, Kanatzidis MG. Quasilinear dispersion in electronic band structure and high Seebeck coefficient in $CuFeS_2$-based thermoelectric materials. Phys Rev Mater 2020;4:025405. https://doi.org/10.1103/PhysRevMaterials.4.025405.
[57] Takabatake T, Suekuni K, Nakayama T, Kaneshita E. Phonon-glass electron-crystal thermoelectric clathrates: experiments and theory. Rev Mod Phys 2014;86:669. https://doi.org/10.1103/RevModPhys.86.669.
[58] He JQ, Girard SN, Kanatzidis MG, Dravid VP. Microstructure-lattice thermal conductivity correlation in nanostructured $PbTe_{0.7}S_{0.3}$ thermoelectric materials. Adv Funct Mater 2010;20:764–72. https://doi.org/10.1002/adfm.200901905.
[59] Hu L, Wu H, Zhu T, Fu C, He J, Ying P, Zhao X. Tuning multiscale microstructures to enhance thermoelectric performance of n-Type Bismuth-Telluride-based solid solutions. Adv Energy Mater 2015;5:1500411. https://doi.org/10.1002/aenm.201500411.
[60] Chen Z, Jian Z, Li W, Chang Y, Ge B, Hanus R, Yang J, Chen Y, Huang M, Snyder GJ, Pei Y. Lattice dislocations enhancing thermoelectric PbTe in addition to band convergence. Adv Mater 2017;29:1606768. https://doi.org/10.1002/adma.201606768.
[61] Jin Q, Jiang S, Zhao Y, Wang D, Qiu J, Tang DM, Tan J, Sun DM, Hou PX, Chen XQ, Tai K, Gao N, Liu C, Cheng HM, Jiang X. Flexible layer-structured Bi_2Te_3 thermoelectric on a carbon nanotube scaffold. Nat Mater 2019;18:62–8. https://doi.org/10.1038/s41563-018-0217-z.
[62] Tian Y, Jia S, Cava RJ, Zhong R, Schneeloch J, Gu G, Burch KS. Understanding the evolution of anomalous anharmonicity in $Bi_2Te_{3-x}Se_x$. Phys Rev B 2017;95:094104. https://doi.org/10.1103/PhysRevB.95.094104.
[63] Chen X, Zhou HD, Kiswandhi A, Miotkowski I, Chen YP, Sharma PA, Lima Sharma AL, Hekmaty MA, Smirnov D, Jiang Z. Thermal expansion coefficients of Bi_2Se_3 and Sb_2Te_3 crystals from 10 K to 270 K. Appl Phys Lett 2011;99:261912. https://doi.org/10.1063/1.3672198.
[64] Klemens PG. Anharmonic decay of optical phonons. Phys Rev 1966;148:845. https://doi.org/10.1103/PhysRev.148.845.
[65] Tian Y, Osterhoudt GB, Jia S, Cava RJ, Burch KS. Local phonon mode in thermoelectric Bi_2Te_2Se from charge neutral antisites. Appl Phys Lett 2016;108:041911. https://doi.org/10.1063/1.4941022.
[66] Usher S, Srivastava GP. Theoretical study of the anharmonic decay of nonequilibrium LO phonons in semiconductor structures. Phys Rev B 1994;50:14179. https://doi.org/10.1103/PhysRevB.50.14179.
[67] Liu MS, Bursill LA, Prawer S, Beserman R. Temperature dependence of the first-order Raman phonon line of diamond. Phys Rev B 2000;61:3391. https://doi.org/10.1103/PhysRevB.61.3391.
[68] Menendez J, Cardona M. Temperature dependence of the first-order Raman scattering by phonons in Si, Ge, and α-Sn: anharmonic effects. Phys Rev B 1984;29:2051. https://doi.org/10.1103/PhysRevB.29.2051.
[69] Balkanski M, Wallis RF, Haro E. Anharmonic effects in light scattering due to optical phonons in silicon. Phys Rev B 1983;28:1928. https://doi.org/10.1103/PhysRevB.28.1928.
[70] Tang H, Herman IP. Raman microprobe scattering of solid silicon and germanium at the melting temperature. Phys Rev B 1991;43:2299. https://doi.org/10.1103/PhysRevB.43.2299.
[71] Gomis O, Vilaplana R, Manjón FJ, Rodríguez-Hernández P, Pérez-González E, Muñoz A, Kucek V, Drasar C. Lattice dynamics of Sb_2Te_3 at high pressures. Phys Rev B 2011;84:174305. https://doi.org/10.1103/PhysRevB.84.174305.
[72] Wu Z, Chen X, Mu E, Liu Y, Che Z, Dun C, Sun F, Wang X, Zhang Y, Hu Z. Lattice strain enhances thermoelectric properties in Sb_2Te_3/Te heterostructure. Adv Electron Mater 2019;6:1900735. https://doi.org/10.1002/aelm.201900735.
[73] Dieter GE. In: Mechanical metallurgy. third ed. McGraw Hill Education; 2017.
[74] Breumier S, Sao-Joao S, Villani A, Lévesque M, Kermouche G. High strain rate micro-compression for crystal plasticity constitutive law parameters identification. Mater Des 2020;193:108789. https://doi.org/10.1016/j.matdes.2020.108789.

Mr. Subarna Das received his B.Sc. and M.Sc. from University of Calcutta in 2012 and 2014 respectively. He is currently working as a Ph.D. candidate at Department of Physics, University of Calcutta under supervision of Dr. Aritra Banerjee and Dr. S. Bandyopadhyay. His research interest is focused on synthesis and characterization of different binary pnictide chalcogenides based thermoelectric material and strongly correlated systems.

Mr. Pintu Singha is a Ph.D. student in the Department of Physics at University of Calcutta. He received his bachelor degree in Physics from the University of Calcutta in 2013. He obtained his master degree in Physics from University of Calcutta in 2015. His current research interests focus on Synthesize and characterization of pnictide chalcogenides based thermoelectric, magnetic and topological materials.

Prof. V. A. Kulbachinskii is presently working as a Professor at Department of Low Temperature Physics and superconductivity, M.V. Lomonosov Moscow State University, Russia. He received Ph.D. in Physics from M.V. Lomonosov Moscow State University, Russia in 1978 with specialization low temperature Physics. His research interest is focused on study of the quantum oscillation of magnetoresistance (Shubnikov – de Haas effect) in heterostructures, quantum wells, transport and Hall effect in different low dimensional materials with practical applications, investigation and characterization of ZnO based films at low temperatures, superconductivity in fullerides and related materials, thermal variation of thermoelectric properties (Resistivity, Thermopower, Heat conductivity etc) of different materials and composites and magnetic property study.

Dr. V. G. Kytin received Ph.D. in Physics from M.V. Lomonosov Moscow State University, Russia in 1995 with specialization in low temperature Physics. Currently, he is an Assistant Professor at Department of Low Temperature Physics and superconductivity, M.V. Lomonosov Moscow State University, Russia. His research interests include transport in oxides, investigation and characterization of ZnO, In_2O_3 based films at low temperatures, thermal variation of thermoelectric properties (Resistivity, Thermopower, Heat conductivity etc) of different materials and composites, magnetic property study, theory of solids, digital methods in Solid state Physics and Boltzmann equation.

Dr. Gangadhar Das is a Post Doctoral Fellow at Chemistry and Physics of Materials Unit in Jawaharlal Nehru Centre For Advanced Scientific Research, Bangalore, India. He obtained his master degree in Physics from Indian Institute of Technology Madras, Chennai in 2011. He received his Ph.D. in physics from Raja Ramanna Centre for Advanced Technology, Indore, India in 2018. His current research interests focus on X-ray Spectroscopy for novel materials.

Ms. S. Janaky is pursuing PhD in the 'Chemistry and Physics of Materials Unit' of Jawaharlal Nehru Centre for Advanced Scientific Research, Bangalore, where she has already completed her master degree in material science. She has three publications in International peer-reviewed journals in various fields of material science till date. Her work majorly comprises of Raman spectroscopy of various materials like topological insulators, MOFs, thermoelectric systems etc., under extreme conditions of temperature and pressure. She is familiar with high pressure Raman and XRD, and Synchrotron XRD studies.

Dr. A. K. Deb received his doctorate degree in 2007 from Department of Materials Science, Indian Association for the Cultivation of Science, Kolkata, India. Currently he is an Assistant Professor of Physics at Raiganj University, West Bengal, India. He obtained his master degree in Physics from Jadavpur University, Kolkata, India. His research focuses on Experimental Materials Science especially X-ray Powder Diffraction Line Profile analysis.

Dr. Sudip Mukherjee is presently working as Scientist-E at UGC DAE CSR, Mumbai Centre, Mumbai, India. He obtained his Ph.D. degree in 2006 from Jadavpur University, India in the area of magnetic nanostructured materials. His work involved fabrication of new class of materials in which their dielectric constant could be modified by application of both electric and magnetic field. His current research interests are on studying the effects of spin fluctuations, magnetic ordering, and external magnetic field on the dielectric properties of the nanomagnetic materials, strongly correlated systems.

Dr. A. Maignan is presently working as Research Director (exceptional class) at Laboratoire de Cristallograhie et Sciences des Matériaux (CRISMAT), Caen, France. He is also Director of the French National Centre for Technological Research on Materials (CNRT Materiaux), UMS 3318 (CNRS/ENSICAEN/ University of Caen, and University of Le Havre) and Scientific in charge of the Excellence Laboratory EMC3 (energy materials and clean combustion center), France. He received his P.hD. in Sciences in 1988 from University of Caen, France. His research interest deals with the research of new materials and the study of structure - property relationships, focusing mainly on functionalities in the energy field: research of new materials for ionic conductors, multiferroic materials, thermoelectric materials etc.

Dr. S. Hebert is currently working as a Senior Researcher at Laboratoire de Cristallograhie et Sciences des Matériaux (CRISMAT), Caen, France. She did her Ph.D. at the CRISMAT laboratory (1995–1998). Since 2015, she is the group leader of the 'New materials: from fundamentals to functionalities' group from CRISMAT, France. Her research interest is based on thermoelectric properties of transition metal oxides and chalcogenides.

Dr. R. Daou received Ph.D. in Physics from University of Cambridge, England in 2005. Currently, he is working as Chargé de Recherche at Laboratoire de Cristallograhie et Sciences des Matériaux (CRISMAT), Caen, France. His research interests include thermoelectric transport in quantum materials, high-resolution measurements in very high magnetic fields, growth and characterisation of new materials for fundamental science and potential thermoelectric applications, with a focus on metallic oxides and sulphides.

Prof. Chandrabhas Narayana is a professor at Jawaharlal Nehru Centre For Advanced Scientific Research (JNCASR), Bangalore, India. He received his Ph.D. in physics from the Indian Institute of Science, Bangalore, India and went on to do Post-Doctoral Research at Cornell University, Ithaca, New York, USA in the Department of Materials Science and Engineering. He has been a part of the Chemistry and Physics of Materials Unit, JNCASR, from 1998. He is working in interdisciplinary areas of Physics, Chemistry and Biology. His main research interests are Brillouin, Raman scattering and materials properties.

Dr. S. Bandyopadhyay is currently working as Associate Professor at Department of Physics, University of Calcutta. He received his M.Sc. in Physics at University of Calcutta in 1996 and Ph.D. in 2002 performing research at Indian Association for the Cultivation of Science, Kolkata, India. His research interest is focused on Transition and Rare earth based Magnetic and Metamagnetic Compounds, Magneto-electric Compounds, Dilute Magnetic Semiconductor (Oxide Semiconductor) and Thermoelectric Materials.

Dr. Aritra Banerjee is currently working as Assistant Professor at Department of Physics, University of Calcutta. He received his M.Sc. in Physics at University of Calcutta in 1998 and did his Ph.D. at Indian Association for the Cultivation of Science, Kolkata, India (1998–2003). Before joining Department of Physics, University of Calcutta as Assistant Professor, he worked as Scientific Officer-D at Indira Gandhi Center for Atomic Research, Kalpakkam, India. His research area is based on study of transport, magnetotransport and magnetic property of thermoelectric material and ZnO based dilute magnetic semiconductors.